Signature for the existence of eta-mesic nucleus

L. C. Liu and Q. Haider
Los Alamos National Laboratory, Los Alamos, New Mexico 87545
(Received 14 April 1986)

It is shown that strongly-bound η-nucleus systems, which we term *η-mesic nuclei*, can be formed between an η meson and nuclei of mass number $A > 10$. We show that a distinct experimental signature for the formation of the η-mesic nucleus can be observed in (π^+,p) reactions. The formation cross sections are predicted. Effects of higher order dynamics on the predicted width of the η-mesic nucleus are also estimated.

I. INTRODUCTION

There are currently extensive theoretical and experimental efforts devoted towards achieving a better understanding of the η and η' mesons. As we know, their observed masses cannot be fully explained in terms of the standard SU(6) model.[1] The η-η' mixing[2] and the isospin breaking π^0-η mixing[3] are also among the many interesting problems pertaining to the eta mesons. We believe that studying η-nucleon interactions can yield additional important information on the nature of the η meson. Because it is nearly impossible to produce an η beam, the nucleus provides a natural laboratory for such investigations.

In recent years, a significant amount of pion-induced η production in ^{3}He, ^{7}Li, and ^{12}C at pion kinetic energies near 500 MeV has been detected at LAMPF.[4] Production of η mesons has also been observed in proton-nucleus collisions[5] at proton kinetic energies around 1 GeV. Studying η-nucleon interactions by means of nuclear reactions has, therefore, become a reality with modern accelerator facilities. Using a coupled-channel model, Bhalerao and Liu[6] have shown that pionic η production on a nucleon in the threshold region proceeds mainly through the formation of the $N^*(1535)$ $(S11)$ resonance and that the $\eta\mathrm{N}N^*$ coupling constant is not small. Their model also predicts an attractive low-energy ηN interaction. A more recent theoretical study[7] further indicates that this attractive ηN interaction can lead to the formation of nuclear bound states of the η meson in nuclei having mass number $A > 10$. Such a bound system, termed the η-mesic nucleus, is caused by the strong interaction between the η meson and all the nucleons in the nucleus.

A novel feature of η-mesic nuclei that distinguishes them from other nuclear bound systems known to date is that these are bound systems constituted of a meson and a nucleus. Furthermore, unlike mesic atoms, mesic nuclei are solely the result of strong interactions. It is worth mentioning that the existence of a mesic nucleus cannot be readily investigated with pions or kaons. Owing to the strong cancellation between the isospin $\frac{1}{2}$ and $\frac{3}{2}$ πN s-wave scattering lengths, the resultant low-energy s-wave pion-nucleus interaction is weak (and repulsive). Although the p-wave pion-nucleus interaction is attractive, its strength depends critically on the local pion momentum that theoretical estimates indicate is very small.[8] The K^+ meson is not suitable because the K^+N interaction is repulsive at low energies. Although the low-energy K^-N interaction is attractive, the use of a stopped K^- beam could be hampered by the presence of large Coulomb interactions that would cause K^- to form preferentially the mesic atoms. On the other hand, because of strangeness conservation, K^- can be produced in medium-energy nuclear reactions only through $\mathrm{K}^+\mathrm{K}^-$ pair production that has a very small cross section. Another advantage associated with the η meson is that the fundamental $\pi\mathrm{N}\rightarrow\eta\mathrm{N}$ interaction is a two-body to two-body process. This latter kinematic feature facilitates the search for η-mesic nuclei by means of two-body to two-body nuclear reactions. In this paper, we study one such reaction. We shall present the calculated cross sections for the formation of an η-mesic nucleus and discuss the associated experimental signature.

In the past, useful information about hadron-nucleon interactions has been obtained through studies of hadron-nucleus bound states.[9–13] Such studies are especially rewarding for those hadrons from which it is nearly impossible to produce beams in the laboratory. In a similar manner, the experimental confirmation of the existence of an η-mesic nucleus will lead to new possibilities of studying the interaction between a nucleon and the short-lived ($\sim 10^{-18}$ s) η meson. For example, because the η-nucleon interaction proceeds mainly through the $N^*(1535)$ resonance, analysis of the discrete energy spectrum of an η-mesic nucleus will allow an accurate determination of the $\eta\mathrm{N}N^*$ coupling constant. Additionally, because of the specific quantum numbers of the η meson, η-mesic nuclei can be used as vehicles to access many new nuclear states that otherwise cannot be easily reached. We, therefore, believe that both theoretical and experimental studies of η-mesic nuclei may produce interesting surprises and have an impact on the future direction of medium-energy physics.

In Sec. II we briefly review the theory of the η-mesic nucleus and make an order of magnitude estimate of the effects on calculated binding energies and widths arising from various simple medium corrections. We present in Sec. III a theoretical framework for the calculation of the formation cross sections of η-mesic nuclei in (π^+,p) reactions. The experimental signature of η-mesic nuclei and

the physics that can be learned from the angular and energy dependences of these cross sections is also discussed. A summary and conclusions are presented in Sec. IV.

II. THEORY OF THE η-MESIC NUCLEUS

A. Covariant η-nucleus optical potential

We use the following momentum-space relativistic three-dimensional integral equation[14] to study η-nucleus systems:

$$\frac{\mathbf{k}'^2}{2\mu}\tilde{\psi}(\mathbf{k}')+\int d\mathbf{k}\langle\mathbf{k}'\,|\,\tilde{V}\,|\,\mathbf{k}\rangle\tilde{\psi}(\mathbf{k})=E\tilde{\psi}(\mathbf{k}')\,, \tag{2.1}$$

where $\tilde{V}$ is the η-nucleus optical potential, $E=\kappa^2/2\mu$ is the (complex) eigenenergy of the system, and $\mu=M_\eta M_A/(M_\eta+M_A)$ is the reduced mass. For bound states, we have $\mathrm{Re}\kappa^2\equiv\kappa_r^2<0$. In spite of its Schrödinger-type form, Eq. (2.1) is covariant. The three-dimensional relativistic wave function $\tilde{\psi}$ and the covariant potential $\langle\mathbf{k}'\,|\,\tilde{V}\,|\,\mathbf{k}\rangle$ are defined by[14]

$$\tilde{\psi}(\mathbf{k})=\left[\frac{R(\kappa_r^2)}{R(k^2)}\right]^{1/2}\psi[\mathbf{k},k^0=W-E_A(\mathbf{k})] \tag{2.2}$$

and

$$\langle\mathbf{k}'\,|\,\tilde{V}\,|\,\mathbf{k}\rangle=R^{1/2}(\mathbf{k}'^2)\langle\mathbf{k}'\,|\,V[W,k'^0=W-E_A(\mathbf{k}'),k^0=W-E_A(\mathbf{k})]\,|\,\mathbf{k}\rangle R^{1/2}(\mathbf{k}^2)\,. \tag{2.3}$$

Here $W=(M_\eta^2+\kappa_r^2)^{1/2}+(M_A^2+\kappa_r^2)^{1/2}$ and $R(\mathbf{k}^2)=(M_\eta+M_A)/[E_\eta(\mathbf{k})+E_A(\mathbf{k})]$. The restriction of the zeroth component of the four-momenta k and k', respectively, to $k^0=W-E_A(\mathbf{k})$ and $k'^0=W-E_A(\mathbf{k}')$ in ψ and V specifies the covariant reduction scheme that led to the relativistic wave equation we are using. The main advantage of working with a covariant theory is that the η-nucleus interaction V can be related to the elementary ηN process by unambiguous kinematical transformations.[15]

The first-order η-nucleus optical potential $\langle\mathbf{k}'\,|\,V\,|\,\mathbf{k}\rangle$ has the form

$$\langle\mathbf{k}'\,|\,V\,|\,\mathbf{k}\rangle=\sum_j\int d\mathbf{Q}\langle\mathbf{k}',-(\mathbf{k}'+\mathbf{Q})\,|\,t(\sqrt{s_j})_{\eta\mathrm{N}\to\eta\mathrm{N}}\,|\,\mathbf{k},-(\mathbf{k}+\mathbf{Q})\rangle\phi_j^*(-\mathbf{k}'-\mathbf{Q})\phi_j(-\mathbf{k}-\mathbf{Q})\,, \tag{2.4}$$

where $\mathbf{k}$ and $\mathbf{k}'$ are, respectively, the initial and final η momenta in the η-nucleus c.m. frame. In Eq. (2.4), the off-shell η-nucleon scattering amplitude $t_{\eta\mathrm{N}\to\eta\mathrm{N}}$ is weighted by the product of the nuclear wave functions $\phi_j^*\phi_j$ corresponding to having the nucleon j at the momenta $-(\mathbf{k}+\mathbf{Q})$ and $-(\mathbf{k}'+\mathbf{Q})$ before and after the collision, respectively. The $\sqrt{s_j}$ is the ηN invariant mass and is equal to the total energy in the c.m. frame of the η and the nucleon j. It is given by

$$\sqrt{s_j}=[\{W-E_{C,j}(\mathbf{Q})\}^2-\mathbf{Q}^2]^{1/2}\simeq M_\eta+M_\mathrm{N}-|\,\epsilon_j\,|-\frac{\mathbf{Q}^2}{2M_{C,j}}\left[\frac{M_\eta+M_A}{M_\eta+M_\mathrm{N}}\right], \tag{2.5}$$

where $E_{C,j}$ and $M_{C,j}$ are, respectively, the total energy and mass of the core nucleus obtained from removing a nucleon j of momentum $-(\mathbf{k}+\mathbf{Q})$ and binding energy $|\,\epsilon_j\,|$. We note from Eqs. (2.4) and (2.5) that the calculation of V involves full off-shell kinematics, in which integration over the Fermi motion variable $\mathbf{Q}$ is carried out. Further, the basic interaction $t_{\eta\mathrm{N}\to\eta\mathrm{N}}$ is always evaluated at subthreshold energies, namely, $\sqrt{s_j}\equiv M_\eta+M_\mathrm{N}-d(\,|\,\epsilon_j\,|\,,\mathbf{Q}^2)$. However, because the thresholds for $\eta\mathrm{N}\to\pi\mathrm{N}$ and $\eta\mathrm{N}\to\pi\pi\mathrm{N}$ reactions are lower than the threshold for $\eta\mathrm{N}\to\eta\mathrm{N}$ scattering, $t_{\eta\mathrm{N}\to\eta\mathrm{N}}$ is still complex.

It is useful to express $t_{\eta\mathrm{N}\to\eta\mathrm{N}}$ in terms of the scattering amplitude $\mathscr{A}$ defined in the ηN c.m. frame:

$$\langle\mathbf{k}',-(\mathbf{k}'+\mathbf{Q})\,|\,t(\sqrt{s_j})_{\eta\mathrm{N}\to\eta\mathrm{N}}\,|\,\mathbf{k},-(\mathbf{k}+\mathbf{Q})\rangle=-\frac{\sqrt{s_j}}{(2\pi)^2}\frac{\mathscr{A}(\sqrt{s_j},\mathbf{p}',\mathbf{p})}{[E_\eta(\mathbf{k}')E_\mathrm{N}(\mathbf{k}')E_\eta(\mathbf{k})E_\mathrm{N}(\mathbf{k})]^{1/2}}\,, \tag{2.6}$$

where $\mathbf{p}$ and $\mathbf{p}'$ denote the relative momenta in the ηN c.m. frame. One can parametrize $\mathscr{A}$ as[6]

$$\begin{aligned}\mathscr{A}(\sqrt{s_j},\mathbf{p}',\mathbf{p})&=K_{p'p}\sum_l A_l(\sqrt{s_j})[u_l(\,|\,\mathbf{p}'\,|\,/\Lambda)u_l(\,|\,\mathbf{p}\,|\,/\Lambda)]^{1/2}\\&\times\left[\frac{\Lambda^2}{\Lambda^2+\mathbf{p}'^2}\right]\left[\frac{\Lambda^2}{\Lambda^2+\mathbf{p}^2}\right](\,|\,\mathbf{p}'\,|\,|\mathbf{p}\,|\,)^l[f_{J,l}-i\sigma(\hat{\mathbf{p}}\times\hat{\mathbf{p}}')g_{J,l}]P_l(z)\\&\equiv F(\sqrt{s_j},\mathbf{p}',\mathbf{p})-i\sigma(\hat{\mathbf{p}}\times\hat{\mathbf{p}}')G(\sqrt{s_j},\mathbf{p}',\mathbf{p})\,,\end{aligned} \tag{2.7}$$

where

$$K_{p'p}=-(\pi/\sqrt{s_j})[E_\eta(\mathbf{p}')E_\mathrm{N}(\mathbf{p}')E_\eta(\mathbf{p})E_\mathrm{N}(\mathbf{p})]^{1/2},\quad z\equiv\hat{\mathbf{p}}'\cdot\hat{\mathbf{p}}\,,$$

and

$$A_l(\sqrt{s_j})=(g_{\eta\mathrm{N}\alpha}^2/2\sqrt{s_j})[\sqrt{s_j}-M_\alpha-\Sigma_\eta^\alpha(\sqrt{s_j})-\Sigma_\pi^\alpha(\sqrt{s_j})-\Sigma_{2\pi}^\alpha(\sqrt{s_j})]^{-1}\,. \tag{2.8}$$

The F and G are, therefore, the spin-nonflip and spin-flip amplitudes. For a spin-zero nucleus, the contribution from the spin-flip amplitude G, when summed over all the target nucleons, becomes zero. The J and l are, respectively, the total and orbital angular momenta of the ηN system. Using the standard angular momentum projector method, one can show that for $J=l+\frac{1}{2}$, one has $f_{J,l}=l+1$ and $g_{J,l}=d/dz$, and that for $J=l-\frac{1}{2}$, one has $f_{J,l}=l$ and $g_{j,l}=-d/dz$. P_l is the Legendre polynomial of order l. The quantities $\sqrt{s_j}$, $\mathbf{p}'$, $\mathbf{p}$, and $\hat{\mathbf{p}}'\cdot\hat{\mathbf{p}}$ can be calculated from $\mathbf{k}'$, $\mathbf{k}$, and $\mathbf{Q}$ using the well-established Lorentz transformations.[15]

The correct low-momentum behavior of the ηN interaction is ensured by the quantity

$$(|\mathbf{p}'||\mathbf{p}|)^l[u_l(|\mathbf{p}'|/\Lambda)u_l(|\mathbf{p}|/\Lambda)]^{1/2}$$

which, for $|\mathbf{p}'|=|\mathbf{p}|$, becomes the well-known penetration factor[16] $|\mathbf{p}|^{2l}u_l$. As noted in Refs. 6 and 7, for low-energy ηN scattering, only the channels with $(l,J)=(0,\frac{1}{2})$, $(1,\frac{1}{2})$, and $(2,\frac{3}{2})$ need to be considered. Furthermore, only one N^* isobar (labeled α) in each of these channels is important; they are the $N^*(1535)$ ($S11$), $N^*(1440)$ ($P11$), and $N^*(1520)$ ($D13$). The quantities Σ_η^α, Σ_π^α, and $\Sigma_{2\pi}^\alpha$ in Eq. (2.8) are the self-energies of the isobar α associated, respectively, with the coupling to the ηN, πN, and $\pi\pi$N intermediate states. We refer to Ref. 6 for the physical meanings of these self-energies and for the values of the coupling constants $g_{\eta N\alpha}$, the range parameters Λ, and the bare isobar mass M_α.

B. η-nucleus bound states

After partial wave decomposition and angular momentum projection, Eq. (2.1) becomes, in general, a system of coupled radial integral equations. It is instructive to first consider spinless nuclei for which the radial integral equations are uncoupled from one another and each depends only on the orbital angular momentum L of the η-nucleus system. We have looked for bound-state solutions corresponding to $\mathrm{Re}E<0$ for six spin-zero nuclei—^{12}C, ^{16}O, ^{26}Mg, ^{40}Ca, ^{90}Zr, and ^{208}Pb. The binding energies and half-widths predicted by the full off-shell calculation, Eqs. (2.4)—(2.8), are summarized in Table I.[17] The solutions labeled set 1 and set 2 are obtained with the ηN interaction parameters $g_{\eta N\alpha}$, M_α, and Λ determined in Ref. 6 from the πN phase shifts of Arndt *et al.* and the CERN theoretical fit, respectively. The nuclear wave functions ϕ_j in Eq. (2.4) were derived from the expermental charge form factors with the proton finite size corrected for.[18–20]

We note from Table I that the number of bound states increases with the nuclear size. The binding energy and the width of a given bound state (e.g., the $1s$ or $1p$ state) also increase with the nuclear size. In ^{208}Pb, we have found four bound states, while for ^{12}C only one loosely-bound state is obtained. For nuclei with mass number $A\leq 10$, no bound-state solutions could be obtained. The fact that a nucleus of sufficient size is required to develop bound states of η that are absent in fewer-nucleon systems is a direct consequence of basic quantum mechanical principles for the existence of bound states. A detailed discussion about this aspect is given in Ref. 7.

We also note from Table I that the states predicted by set 1 are systematically more deeply bound than those predicted by set 2. Since the ηN interactions that have led to these two sets of solutions give nearly identical ηN scattering lengths, $a_0=(0.28+0.19i)$ and $(0.27+0.22i)$ fm, respectively,[6] we conclude that the difference in the binding energies reflects the sensitivity of the bound-state formation to the off-shell behavior of the ηN interaction, in particular, to the very different range parameters Λ of these two sets of ηN interactions.

We have further noted that the exclusion of p- and d-wave ηN interactions from Eq. (2.7) has negligible effects on the predicted binding energies and widths. This is a direct consequence of the correct low-momentum behavior of the ηN interaction model. This insignificance of the p- and d-wave interactions greatly simplifies the theoretical calculation of η-nucleus bound states for nu-

TABLE I. Binding energies and half-widths (both in MeV) of various η-mesic nuclei given by the full off-shell calculation.

Nucleus	Orbital	Set 1	Set 2
^{208}Pb	$1s$	$-(18.46+10.11i)$	$-(16.23+9.90i)$
	$2s$	$-(2.37+5.82i)$	$-(0.67+5.26i)$
	$1p$	$-(12.28+9.28i)$	$-(9.88+8.84i)$
	$1d$	$-(3.99+6.90i)$	$-(2.06+6.44i)$
^{90}Zr	$1s$	$-(14.80+8.87i)$	$-(12.59+8.56)$
	$1p$	$-(4.75+6.70i)$	$-(2.90+6.01i)$
^{40}Ca	$1s$	$-(8.91+6.80i)$	$-(6.88+6.16i)$
^{26}Mg	$1s$	$-(6.39+6.60i)$	$-(4.62+5.94i)$
^{16}O	$1s$	$-(3.45+5.38i)$	$-(1.87+4.48i)$
^{12}C	$1s$	$-(1.19+3.67i)$	$-(0.09+2.80i)$

clei with spin. For example, the spin-orbit η-nucleus interaction, which arises from the p- and d-wave ηN interactions, can be neglected in bound-state calculations.

C. Effects of higher-order dynamics

It is known that the second-order, density-squared (ρ^2) dependent pion-nucleus optical potential, arising from true pion absorption on two nucleons [Fig. 1(a)], is very important. In the following, we briefly examine the possibilities of η absorption in the η-nucleus interaction. Contributions to the second-order, ρ^2-dependent η-nucleus optical potential by true η absorption are illustrated in Figs. 1(b) and 1(c). Figure 1(b) corresponds to an η absorption after ηN scattering. Figure 1(c) corresponds to an "indirect" η absorption in the sense that the η is first converted to a high-energy ($\simeq 3M_\pi$) pion that is subsequently absorbed. The absorption process of Fig. 1(b) is strongly suppressed by the dynamical effect that the ηNN coupling constant [at the lower vertices in Fig. 1(b)] is extremely small. (See Ref. 6 for a more detailed discussion.) The process of Fig. 1(c) is much more complex, and no reliable estimates can be made concerning its effects on the widths and shifts. Detailed microscopic calculation of Fig. 1(c) is called for in future studies. The absorption of η by many nucleons may also play some role. However, we believe that the likelihood of such processes rapidly decreases with the increase of the orders of multiple scattering that precedes the absorption. Consequently, we did not consider η absorption in the present work.

Another η-nucleus dynamics that can lead to a higher-order density-dependent η-nucleus potential is the nuclear medium effect on the basic ηN interaction. These medium effects modify the N^* self-energies and, thereby, the η-nucleus potential V. They are represented in Fig. 2 by the bubble insertions of the intermediate meson and nucleon lines of the self-energies. While the open bubble on the nucleon lines can be caused by Pauli blocking as well as by the scattering of the nucleon from the other target nucleons, the shaded and filled bubbles on the meson lines are due mainly to meson scattering from the other nucleons. These rescatterings modify the propagators of the particles.

To provide an order of magnitude estimate of these effects, we have evaluated Pauli blocking effects on N^* self-energies by using a Fermi gas model for the nucleus[21] and found that they amount to reducing Im(V) by $\sim 5\%$ and cause a very small change in Re(V). We refer to Ref. 7 for the cause of small Pauli blocking effects in the η-nucleus system. We have also estimated the modifications of propagators in Fig. 2 by using Eq. (3.1) of Ref. 22. In these calculations, the forward η-, π-, and N-nucleus scattering amplitudes that are used to "dress" the intermediate mesons and nucleons are obtained from the respective first-order optical potentials [i.e., Eq. (2.4), Ref. 23, and Refs. 24 and 25]. We have noted that the propagator modifications alone increase Im(V) by $\sim 5\%$. When both the Pauli blocking and propagator modifications are included, Im(V) is nearly unchanged, while Re(V) reduces by less than 6%. Compared to the results given in Table I, these corrections result in an insignificant change in the calculated half-widths and a decrease in the calculated binding energies (by ~ 0.4 MeV in ^{12}C to ~ 0.6 MeV in ^{16}O). Consequently, with these estimated medium modifications, the set 2 interaction will not give rise to a bound-state solution to ^{12}C.

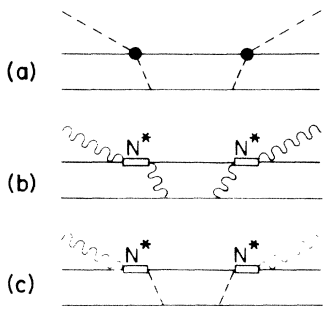

FIG. 1. Contributions to the second-order pion-nucleus or η-nucleus optical potential from two-nucleon meson absorption: (a) pion absorption; (b) η absorption; and (c) "indirect" η absorption (see the text).

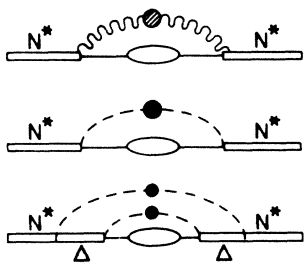

FIG. 2. Self-energies of N^* in the nuclear medium. The solid, dashed, and wavy lines denote, respectively, the nucleon, the pion, and the η. The open, shaded, and filled ovals denote the medium corrections discussed in the text.

In summary, our estimates indicate that absorption and medium effects introduce modifications of the order of ~ 1 MeV to the binding energies and widths. Although more elaborate calculations are clearly necessary, microscopic evaluation of absorption and medium effects is, however, beyond the scope of this paper because it will involve at least a three-body calculation in a finite nucleus. Such calculations are called for when experimental data become available. We have, however, noted from our cross-section calculations (Sec. III) that so long as a bound state can exist, the calculated results are not very sensitive to the binding energy of the η. Because the purpose of this work is to identify the signature for the existence of the η-mesic nucleus, these higher-order effects will not be included in the calculations. The readers are, therefore, advised to regard the values given in Table I as an order-of-magnitude estimate.

III. FORMATION OF AN η-MESIC NUCLEUS IN NUCLEAR REACTIONS

As our calculations have indicated, in most cases the η is bound in low-lying orbitals (Table I). The probability of having an η in these orbitals is peaked at low momenta.

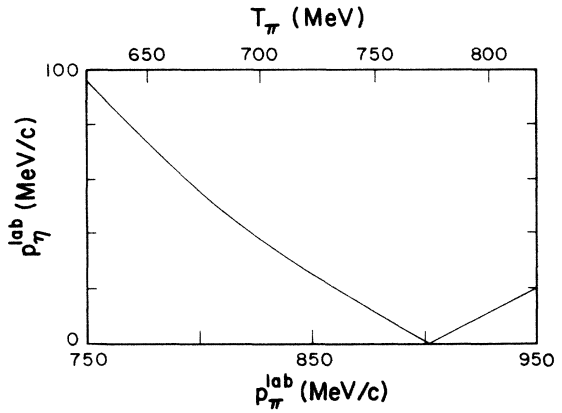

FIG. 3. The lowest η momentum produced in the free $\pi^+ n \to \eta p$ reaction as a function of the pion beam momentum.

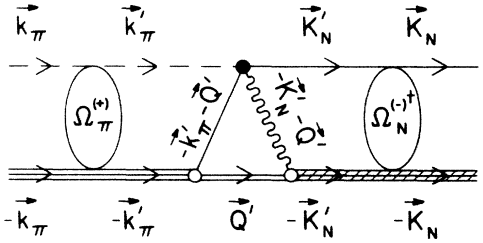

FIG. 4. Diagram for the formation of the η-mesic nucleus via the reaction ${}^Z A(\pi^+,p)^Z_\eta B$. The pion, the nucleon, the η meson, the nuclei, and the mesic nucleus are denoted by the dashed, thin-solid, wavy, multiple, and shaded lines, respectively. The filled circle is the $\pi N \to \eta N$ amplitude while the open circles are the nuclear vertices. The Ω's are the wave operators.

Consequently, the production of a low-momentum η meson will favor the formation of an η-mesic nucleus. On the other hand, because of the kinematics of the two-body $\pi N \to \eta N$ reaction, a low-momentum η is necessarily associated with a high-momentum nucleon in the laboratory frame. However, the lowest momentum an η can have depends strongly on the initial pion energy. We illustrate this latter feature in Fig. 3. As in the case of the $KN \to \Lambda\pi$ reaction, there is also in the free $\pi N \to \eta N$ reaction a "magic" incoming projectile momentum (~ 900 MeV/c) at which the η is produced at rest. From the above heuristic analysis, we conclude that the reaction ${}^Z A(\pi^+,p)^Z_\eta B$ leading to the emission of a high-energy outgoing proton is favorable to the search for the η-mesic nucleus. In this reaction kinematics, the η meson is produced at low momenta. A distinct peak in the outgoing proton energy spectrum will then constitute the signature for the formation of the η-mesic nucleus ${}^Z_\eta B$.

A. The ${}^Z A(\pi^+,p)^Z_\eta B$ reaction

We consider the reaction mechanism of Fig. 4, which corresponds to a distorted-wave impulse approximation (DWIA) to the process

$$\pi^+ + {}^Z A \to p + [\eta + {}^Z(A-1)] = p + {}^Z_\eta B \ .$$

In terms of the kinematic variables defined in Fig. 4, the differential cross sections for the formation of the η-mesic nucleus are

$$\frac{d\sigma}{d\Omega} = \frac{(2\pi)^4}{(2J_A+1)} \frac{\mu_\pi}{|\mathbf{k}_\pi|} \sum_{m'_s \nu_A \nu_B} \left| \sum_{jm_j} (\mathcal{N}_j \mu_N | \mathbf{K}_N |)^{1/2} \right.$$
$$\times \int d\mathbf{K}'_N d\mathbf{k}'_\pi \Psi^{*(-)}_{W'}(\mathbf{K}'_N) \Phi^{(+)}_{W'}(\mathbf{k}'_\pi)$$
$$\left. \times [(2\pi)^3 \langle \mathbf{K}'_N, \tfrac{1}{2} t'_N = \tfrac{1}{2}, \tfrac{1}{2} m'_s; -\mathbf{K}'_N, T_B t_B, J_B \nu_B | A_{\eta\pi} | \mathbf{k}'_\pi, 1 t_\pi = 1; -\mathbf{k}'_\pi, T_A t_A, J_A \nu_A \rangle] \right|^2 , \quad (3.1)$$

where the subscript N refers to the outgoing proton in the (π^+,p) reactions considered here. $\Psi^{*(-)}$, $\Phi^{(+)}$, and $A_{\eta\pi}$ denote, respectively, the distorted waves of the proton and the pion, and the nuclear pionic η production amplitude. The notation for the quantum numbers of a particle labeled i is such that $(T_i t_i)$ and $(J_i \nu_i)$ denote, respectively, the isospin and its z component, and the spin and its z component. For the initial (bound) nucleon, we shall adopt the shell-model notation: $(l m_l, \frac{1}{2} m_s) j m_j$. The z component of the spin of the final proton is denoted by m'_s. The factor $\mathcal{N}_j$ arises from the antisymmetrization of nucleons and is equal to the number of bound nucleons in the shell j of the target nucleus. For a closed shell, we have $\mathcal{N}_j = 2(2j+1)$.

The total c.m. energy of the pion-nucleus system is given by

$$W' = [(M_\pi + M_A)^2 + 2T^{lab}_\pi M_A]^{1/2} . \quad (3.2)$$

The initial and final relative c.m. momenta are, respectively,

$$|\mathbf{k}_\pi| = \frac{1}{2W'} [\{W'^2 - (M_\pi + M_A)^2\} \times \{W'^2 - (M_\pi - M_A)^2\}]^{1/2} \quad (3.3)$$

and

$$|\mathbf{K}_N| = \frac{1}{2W'} [\{W'^2 - (M_N + M_{B,j})^2\} \times \{W'^2 - (M_N - M_{B,j})^2\}]^{1/2} . \quad (3.4)$$

In Eq. (3.4)

$$M_{B,j}=M_{C,j}+M_\eta-|\mathrm{Re}E_\eta|\ , \tag{3.5}$$

where $M_{C,j}$ is the mass of the residual nucleus obtained after removing a j-shell nucleon from the target nucleus, and $|\mathrm{Re}E_\eta|$ is the binding energy of the η. Consequently, $\mathbf{K}_N$ depends on the particular shell from which the nucleon is ejected. (For brevity, the j dependence of K_N will not be written explicitly.) The reduced "masses" appearing in Eq. (3.1) are defined as

$$\mu_\pi=E_\pi(\mathbf{k}_\pi)E_A(\mathbf{k}_\pi)/W'$$

and

$$\mu_N=E_N(\mathbf{K}_N)E_B(\mathbf{K}_N)/W'\ .$$

The nuclear transition amplitude $A_{\eta\pi}$ in Eq. (3.1) is a functional of the off-shell $\pi N\to\eta N$ t matrix $t(\sqrt{s_j})_{\pi N\to\eta N}$, where $\sqrt{s_j}$ is defined as in Eq. (2.5) with $\mathbf{Q}$ replaced by $\mathbf{Q}'$ (see Fig. 4). We refer to the Appendix for details of the cross section calculations.

If one measures the outgoing protons with an energy resolution better than or equal to Γ_η (the width of the mesic nucleus ${}_\eta B$), one can then isolate experimentally the contributions to $d\sigma/d\Omega$ from the neutrons belonging to the shells whose binding energies differ from one another by more than Γ_η. Consequently, only a few values of j need to be included in the summation in Eq. (3.1). One further notes that for spin-zero ($J_A=0$) target nuclei, the cross section [Eq. (A4)] is simply given by[26]

$$\frac{d\sigma}{d\Omega}=\frac{(2\pi)^4\mu_\pi}{|\mathbf{k}_\pi|}\sum_{jlm_lLm_L}(2j+1)\mu_N|\mathbf{K}_N|(|\tilde{F}|^2+|\tilde{G}|^2\sin^2\theta)|(2l+1)^{-1/2}I^{\mathrm{EDW}}_{Lm_L,lm_l}|^2\ , \tag{3.6}$$

where $\sin^2\theta=1-(\hat{\mathbf{p}}\cdot\hat{\mathbf{p}}')^2$, and the quantities $\tilde{F}$ and $\tilde{G}$, and I^{EDW} are defined, respectively, in Eqs. (A3) and (A6). For example, if one chooses ^{16}O as the target and has an energy resolution of 10 MeV [$\simeq\Gamma({}^{15}_\eta\mathrm{O})$], then because the level spacing between the s and p shells in ^{16}O is $\sim$28 MeV, one can separate the contributions given by the $1p_{3/2}$, $1p_{1/2}$ shells from those given by the $1s_{1/2}$ shell. One important feature of Eq. (3.6) is that the shape of the differential cross sections is characterized by the angular momentum transfers to the nucleus, e.g., $|l-L|$.

B. Calculated η-mesic nucleus formation cross sections

In this subsection, we present the calculated cross sections for the reactions $^{12}\mathrm{C}(\pi^+,\mathrm{p})^{11}_\eta\mathrm{C}$, $^{16}\mathrm{O}(\pi^+,\mathrm{p})^{15}_\eta\mathrm{O}$, $^{26}\mathrm{Mg}(\pi^+,\mathrm{p})^{25}_\eta\mathrm{Mg}$, and $^{40}\mathrm{Ca}(\pi^+,\mathrm{p})^{39}_\eta\mathrm{Ca}$. Because the η is to be captured into the residual nucleus, we list in Table II the binding energies and half-widths of the mesic nuclei ${}^{11}_\eta\mathrm{C}$, ${}^{15}_\eta\mathrm{O}$, ${}^{25}_\eta\mathrm{Mg}$, and ${}^{39}_\eta\mathrm{Ca}$. These results are obtained with the full off-shell calculation, Eqs. (2.4)–(2.8). As we can see, the weaker set 2 $\eta N\to\eta N$ interaction does not give a bound-state solution for ${}^{11}_\eta\mathrm{C}$, whereas the set 1 interaction still predicts the existence of a loosely-bound state. For definiteness, we will use the set 1 interaction in the following cross section calculations.

We present in Fig. 5 the differential cross sections at $p_\pi^{\mathrm{lab}}=740$ MeV/c for the reactions $^{12}\mathrm{C}(\pi^+,\mathrm{p})^{11}_\eta\mathrm{C}$, $^{16}\mathrm{O}(\pi^+,\mathrm{p})^{15}_\eta\mathrm{O}$, $^{26}\mathrm{Mg}(\pi^+,\mathrm{p})^{25}_\eta\mathrm{Mg}$, and $^{40}\mathrm{Ca}(\pi^+,\mathrm{p})^{39}_\eta\mathrm{Ca}$. The corresponding integrated cross sections are 116, 195, 71, and 54 μb. In these calculations, the s-, p-, and d-wave $\pi N\to\eta N$ interactions were all included. As can be seen from the figure, the calculated differential cross sections are all peaked at small outgoing proton angles. This feature can be easily understood because at this incident pion momentum, small proton angles correspond to large proton momenta and small η momenta in the laboratory frame. As discussed at the beginning of Sec. III, small η momenta facilitate the formation of the η-mesic nucleus. Based on the energy-resolution consideration discussed in the preceding section and on the half-widths of the mesic nuclei given in Table II, we included in our calculations

TABLE II. Binding energies and half-widths (both in MeV) of the η-mesic nuclei relevant to this study.

Nucleus	Orbital	Set 1	Set 2
^{39}Ca	$1s$	$-(8.48+6.57i)$	$-(6.52+5.96i)$
^{25}Mg	$1s$	$-(5.79+6.23i)$	$-(4.13+5.59i)$
^{15}O	$1s$	$-(2.65+4.77i)$	$-(1.28+3.94i)$
^{11}C	$1s$	$-(0.46+2.94i)$	no solution

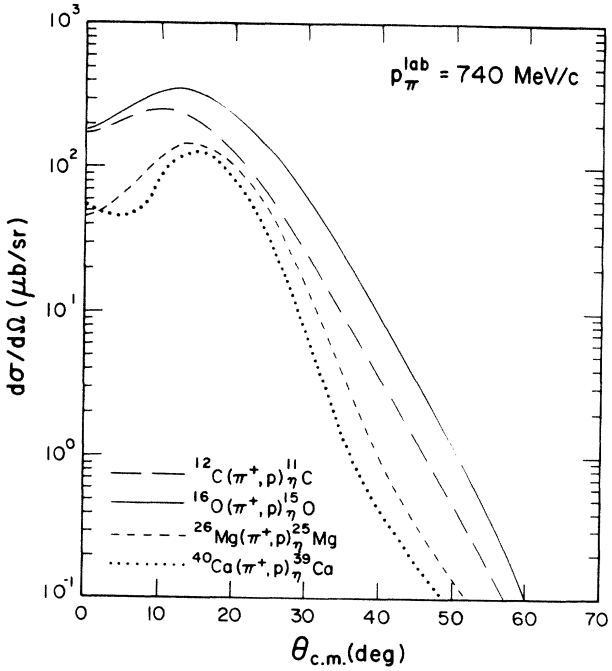

FIG. 5. Calculated differential cross sections for the formation of the η-mesic nucleus at pion beam momentum 740 MeV/c as a function of the outgoing proton angle in the η-nucleus c.m. frame.

the target neutrons of the following shells: $j=\frac{3}{2}$ $(l=1)$ for ^{12}C, $j=\frac{3}{2}$ and $\frac{1}{2}$ $(l=1)$ for ^{16}O, $j=\frac{5}{2}$ $(l=2)$ for ^{26}Mg, and $j=\frac{3}{2}$ $(l=2)$ and $j=\frac{1}{2}$ $(l=0)$ for ^{40}Ca. Because in the corresponding residual nuclei only the $1s$ bound-state of η can exist, it follows that $L=0$ in Eq. (3.6) and that the orbital angular momentum transfers involved in the formation of these η-mesic nuclei are, respectively, $|l-L|=1$, 1, 2, and 2 (and 0). This explains why the peaking of the cross sections occurs at smaller angles in C and O than in Mg and Ca.

Several factors in Eq. (3.6) can affect the magnitude of the small-angle cross sections: (a) the distortions of the incoming pion and the outgoing proton wave functions. The larger the nucleus the stronger is the attenuation of the wave functions. (b) The active neutron number $(2j+1)$ which equals 4, 6, 6, and 6 for C, O, Mg, and Ca, respectively. This factor explains why the cross section for $^{15}_{\eta}$O is greater than for $^{11}_{\eta}$C. (c) The overlap integral I^{EDW} whose magnitude depends on the momentum transfer to the nucleus, which in turn depends on the incident pion energy. We conclude from our calculations that the ^{16}O target represents the most ideal case for an initial search for the η-mesic nucleus.

In Fig. 6, we show the energy dependence of the total cross section for the reaction $^{16}\mathrm{O}(\pi^+,\mathrm{p})^{15}_{\eta}\mathrm{O}$. The solid, long-dashed, and short-dashed curves correspond, respectively, to cross sections obtained with the $(s+p+d)$ waves, $(s+p)$ waves, and s-wave $\pi\mathrm{N}\to\eta\mathrm{N}$ interactions in Eqs. (A3) and (3.6). The differences among these energy dependences indicate that the p- and d-wave $\pi\mathrm{N}\to\eta\mathrm{N}$ interactions are important at these high energies. The cross sections are peaked at $p_\pi^{\mathrm{lab}}\simeq 740$ MeV/c corresponding to a πN invariant mass of about 1520 MeV. This generally reflects the combined effects of the $N^*(1520)$ $(D13)$ and $N^*(1535)$ $(S11)$ resonances. As can be seen from Fig. 5, at this incident pion momentum the main contributions to the integrated cross sections come from $\theta_{\mathrm{p}}\leq 15°$, which, according to our analysis, corresponds to a backward η production angle ($\sim 110°$) in the ηN c.m. frame. In this angular region, the sign of the Legendre polynomials in the production amplitude $\tilde{\mathscr{A}}$ [Eqs. (2.7) and (A3)] makes the sign of the p- and d-wave $\pi\mathrm{N}\to\eta\mathrm{N}$ amplitudes opposite to the sign of the s-wave $\pi\mathrm{N}\to\eta\mathrm{N}$ amplitude. Therefore, at $p_\pi^{\mathrm{lab}}=740$ MeV/c, the inclusion of p- and d-wave ηN interactions reduces the calculated cross sections. The kinematics changes for $p_\pi^{\mathrm{lab}}>780$ MeV/c, where $\theta_{\mathrm{p}}\leq 15°$ correspond to η produced at angles greater than 120° in the ηN c.m. frame. As a result, the s- and p-wave amplitudes have opposite signs while the s- and d-wave amplitudes have the same sign. This leads to a reversal in positions of the solid and long-dashed curves. On the other hand, the kinematics is very different at $p_\pi^{\mathrm{lab}}=620$ MeV/c. At this momentum, $\theta_{\mathrm{p}}\leq 15°$ correspond to η also produced at small angles in the ηN c.m. frame. Consequently, the s-, p- and d-wave amplitudes contribute constructively.

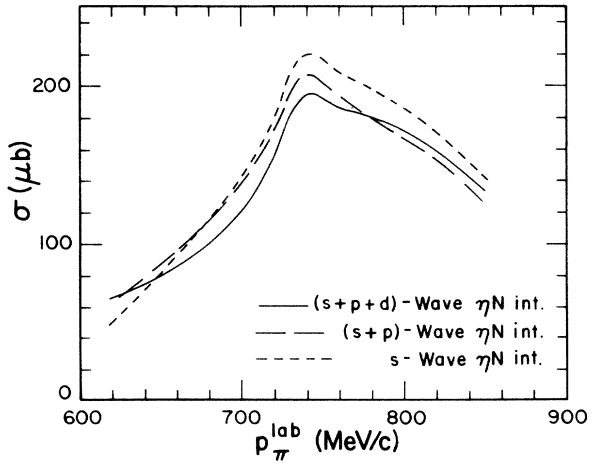

FIG. 6. Integrated cross section for the reaction $^{16}\mathrm{O}(\pi^+,\mathrm{p})^{15}_{\eta}\mathrm{O}$ as a function of the pion beam momentum.

We conclude this section by noting that various energy-dependent factors, such as distortions, the basic $\pi\mathrm{N}\to\eta\mathrm{N}$ kinematics, the N^* resonances in the basic meson-nucleon interaction, and the overlap between the initial nucleon and final η bound-state wave functions can affect the reaction cross section. As a result, the largest mesic nucleus formation cross section occurs at a pion momentum much smaller than the "magic" momentum (~ 900 MeV/c), as a simpler analysis (Fig. 3) would imply.

C. Signature of the η-mesic nucleus

The calculated energy spectrum of the outgoing proton is shown in Fig. 7 for the reaction $^{16}\mathrm{O}(\pi^+,\mathrm{p})^{15}_{\eta}\mathrm{O}$ at $p_\pi^{\mathrm{lab}}=740$ MeV/c and a laboratory proton emission angle $\theta_{\mathrm{p}}^{\mathrm{lab}}=15°$. The peak of ~ 10 MeV width (thin solid curve) at $T_{\mathrm{p}}^{\mathrm{lab}}\simeq 185$ MeV corresponds to the formation of $^{15}_{\eta}$O after the removal of $1p$-shell neutrons in ^{16}O. The area between this peak and the background (thick solid curve) is equal to the differential cross section at $\theta_{\mathrm{c.m.}}\sim 16°$ in

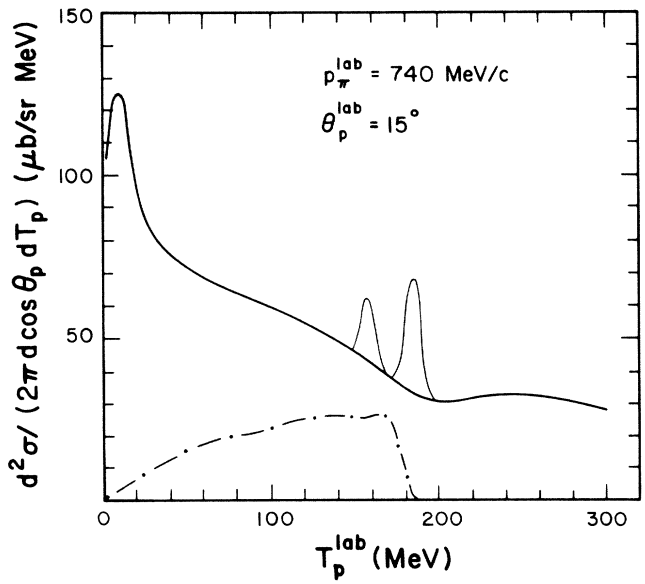

FIG. 7. Calculated cross sections for the reaction $\pi^+ + {}^{16}\mathrm{O}\to\mathrm{p}+X$ at $p_\pi^{\mathrm{lab}}=740$ MeV/c and $\theta_{\mathrm{p}}^{\mathrm{lab}}=15°$ as a function of the outgoing proton kinetic energy in the laboratory frame. The peaks (thin solid curve) correspond to the formation of the η-mesic nucleus $^{15}_{\eta}$O. The thick solid and dot-dashed curves represent, respectively, the background events due to the $(\pi^+,\mathrm{p})X$ and $(\pi^+,\eta\mathrm{p})X$ processes.

Fig. 5. A nearby second peak (thin solid curve) at a lower proton energy ($T_p^{lab} \simeq 157$ MeV) corresponds to the formation of $^{15}_{\eta}$O when $1s$ neutrons are removed from the target.

There are two types of background events. The thick solid curve in Fig. 7 represents the contributions to the reaction ^{16}O(π^+,p)X by the reaction processes that do not involve η production. These processes are quasi-free knockout, multiple-pion and -proton scattering, pion absorption, etc. We calculated this background using the intranuclear cascade code ISOBAR,[27] with the calculated cross section normalized to the total reaction cross section obtained from the pion-nucleus optical potential. Our calculations yield a smooth background of ~ 32 μb/sr MeV at $T_p^{lab} \simeq 185$ MeV. Since the height of the peak that is due to the formation of $^{15}_{\eta}$O is ~ 35 μb/sr MeV, we have a signal-to-background ratio of ~ 1. Indeed, at small proton emission angles the protons of large momenta cannot be caused by direct quasi-knockout. (The probability of finding such a high-momentum nucleon in the nucleus is very small.) Consequently, these high-momentum protons are due mainly to multiple scattering, and the cross sections for these events are low. More interestingly, this lowered background is coupled with an enhanced signal because the η production is peaked in the kinematic region associated with small emerging proton angles. Our analysis indicates, therefore, that detecting protons at small angles is preferable. In Fig. 8, we present this signal-to-background ratio as a function of the pion beam momentum.

The dot-dashed curve in Fig. 7 represents the background contribution given by the reaction ^{16}O(π^+,ηp)X that involves η production but not the formation of the η-mesic nucleus. For any given shell of target neutrons, because of the overall energy-momentum conservation, this background contribution becomes zero at a proton energy that is smaller than the position of the corresponding mesic nucleus peak by an amount equal to the η binding energy. The full background contribution can be obtained by summing the cross sections given by the thick solid and the dot-dashed curves in Fig. 7. It is easy to check that the full background contribution does not mask the existence of both $^{15}_{\eta}$O peaks in the proton spectrum.

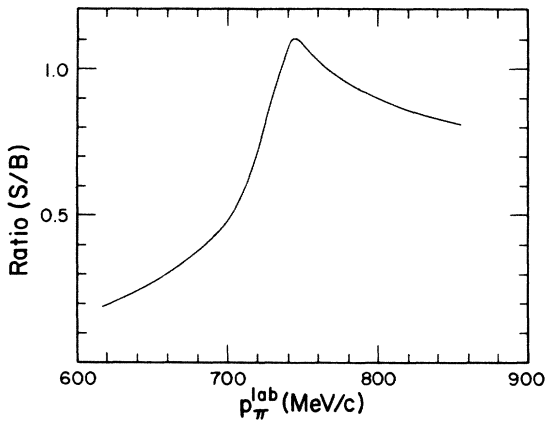

FIG. 8. Dependence on the pion beam momentum of the signal-to-background ratio at $\theta_p^{lab} = 15°$ for the formation of $^{15}_{\eta}$O associated with the removal of $1p$ neutrons.

IV. SUMMARY AND CONCLUSIONS

We have shown that η-nucleus bound states (the η-mesic nucleus) can be formed in ^{15}O and heavier nuclei. Our calculations also indicate that whether or not an η-mesic nucleus can be formed in the border line case with ^{11}C depends critically on the details of the basic ηN interaction. On the other hand, we have also noted that so long as an η bound state can exist, the calculated $^Z A(\pi^+,\mathrm{p})^Z_\eta B$ cross sections are insensitive to these interaction details. Because of this feature, we believe that the predictions given in Sec. III represent a reliable guide to the search for the formation of the η-mesic nucleus in the ^{16}O(π^+,p)$^{15}_{\eta}$O reaction.

In spite of the simple free $\pi\mathrm{N} \rightarrow \eta\mathrm{N}$ kinematics which favors the use of $p_\pi^{lab} \simeq 900$ MeV/c, our calculations indicate that $p_\pi^{lab} \simeq 740$ MeV/c leads to a maximum cross section as well as an optimal signal-to-background ratio (Fig. 8). The fact that the maximum of the cross section occurs at this incident pion momentum is a result of the $N^*(1535)$ ($S11$) resonance and the favorable overlapping between the nucleon and η bound-state wave functions in this energy region.

Finally, we emphasize that experimental confirmation of our predictions will enable an effective investigation of the η-nucleus dynamics. In particular, an accurate determination of η binding energies will yield useful information on the η-nucleon interaction.

ACKNOWLEDGMENTS

We thank Dr. C. B. Dover for helpful discussions. This work was performed under the auspices of the Division of Nuclear Physics, Office of High Energy and Nuclear Physics, U.S. Department of Energy (Contract No. W-7405-ENG-36/8311E551).

APPENDIX

The nuclear transition amplitude $A_{\eta\pi}$ in Eq. (3.1) can be expressed in terms of the off-shell $\pi\mathrm{N} \rightarrow \eta\mathrm{N}$ t matrix ($t_{\pi\mathrm{N}\rightarrow\eta\mathrm{N}}$) as

$$\langle \mathbf{K}'_{\mathrm{N}}, \tfrac{1}{2}t'_{\mathrm{N}} = \tfrac{1}{2}, \tfrac{1}{2}m'_s; -\mathbf{K}'_{\mathrm{N}}, T_B t_B, J_B \nu_B \mid A_{\eta\pi} \mid \mathbf{k}'_\pi, 1t_\pi = 1; -\mathbf{k}'_\pi, T_A t_A, J_A \nu_A \rangle$$

$$= \sum_{\substack{\gamma l m_l m_s \\ J_C \nu_C L m_L}} \mathscr{C} \int d\mathbf{Q}' \psi^*_{Lm_L}(\mathbf{Q}' + \beta\mathbf{K}'_{\mathrm{N}}) \phi_{nlm_l}(\mathbf{Q}' + \alpha\mathbf{k}'_\pi)$$

$$\times \langle -(\mathbf{K}'_{\mathrm{N}} + \mathbf{Q}'); \mathbf{K}'_{\mathrm{N}}, \tfrac{1}{2}t'_{\mathrm{N}} = \tfrac{1}{2}, \tfrac{1}{2}m'_s \mid t(\sqrt{s_j})_{\pi\mathrm{N}\rightarrow\eta\mathrm{N}} \mid \mathbf{k}'_\pi; -(\mathbf{k}'_\pi + \mathbf{Q}'), \tfrac{1}{2}t_{\mathrm{N}} = -\tfrac{1}{2}, \tfrac{1}{2}m_s \rangle \ , \quad \text{(A1)}$$

where $\beta=M_{C,j}/(M_\eta+M_{C,j})$ and $\alpha=(A-1)/A$. The ψ and ϕ are, respectively, the bound-state wave functions of the η and the initial nucleon, with L and m_L denoting the η orbital angular momentum and its projection in the mesic nucleus B. For simplicity of notation, the isospin variables of the π^+ and the η have not been written explicitly and we have also introduced the shorthand notation

$$\mathscr{C}=C^{1/2\ \ T_BT_A}_{-1/2t_B\ t_A}C^{l\ \ 1/2j}_{m_lm_s\ m_j}C^{j\ \ J_CJ_A}_{m_j\nu_C\nu_A}C^{L\ \ J_CJ_B}_{m_L\nu_C\nu_B}f(\gamma;J_CT_C)\ , \tag{A2}$$

with $f(\gamma;J_CT_C)$ denoting the coefficient of fractional parentage (cfp). The Clebsch-Gordan coefficient $C^{1/2\ \ T_BT_A}_{-1/2t_B\ t_A}$ reminds us that only the neutrons in the nucleus A are contributing to the ${}^ZA(\pi^+,\mathrm{p})^Z_\eta B$ reaction.

The parametrization of $t_{\pi N\to\eta N}$ is similar to that for $t_{\eta N\to\eta N}$ in Eqs. (2.6)—(2.8), with the proviso that the c.m. amplitude $\mathscr{A}$ in Eq. (2.6) be replaced by

$$\tilde{\mathscr{A}}(\sqrt{s_j},\mathbf{p}',\mathbf{p})\equiv\tilde{F}(\sqrt{s_j},\mathbf{p}',\mathbf{p})-i\boldsymbol{\sigma}(\hat{\mathbf{p}}\times\hat{\mathbf{p}}')\tilde{G}(\sqrt{s_j},\mathbf{p}',\mathbf{p})\ . \tag{A3}$$

The $\tilde{F}$ and $\tilde{G}$ are analogous to F and G in Eq. (2.7) except that: (a) in the expression for $A_l(\sqrt{s_j})$ [Eq. (2.8)], the coupling constant $g^2_{\eta N\alpha}$ should be replaced by $\sqrt{2/3}g_{\eta N\alpha}g_{\pi N\alpha}$, where the factor $\sqrt{2/3}$ is due to isospin transfer; and (b) the Λ associated with the initial meson-nucleon c.m. momentum $\mathbf{p}$ should be replaced by the corresponding range parameter for $\pi N\alpha$ coupling.[6]

Since we are dealing with a high-momentum incident pion and outgoing proton, the use of eikonal distorted wave functions for $\Psi^{(-)}$ and $\Phi^{(+)}$ represents a good approximation.[28] Because of the basically forward peaking of the particle propagation at high energies, one can also assume that $\mathbf{k}'_\pi$ and $\mathbf{K}'_N$ peak around their asymptotic values $\mathbf{k}_\pi$ and $\mathbf{K}_N$, respectively. It is, therefore, a good approximation to factorize $t_{\pi N\to\eta N}$ out of the $\mathbf{Q}'$ integration and evaluate it at an average $\langle\mathbf{Q}'\rangle=-\alpha\mathbf{k}_\pi$ and at an effective interaction energy $\langle\sqrt{s}\,\rangle=[(M^2_\pi+M^2_N)+2T^{\mathrm{lab}}_\pi M_N]^{1/2}-\delta$. The above choice of $\langle\mathbf{Q}'\rangle$ and $\langle\sqrt{s}\,\rangle$ is based on the considerations that at these high energies, the momentum of the target nucleon can be neglected with respect to the pion momentum. Consequently, we can use the above $\langle\mathbf{Q}'\rangle$ which corresponds to a fixed nucleon. However, because the πN interaction is strongly energy dependent, the dynamical effects of the Fermi motion and nuclear binding should not be neglected. To account for these latter effects, we use a shift of $\delta=30$ MeV.[29]

With the above-mentioned eikonal distorted-wave (EDW) approximation, Eq. (A1) becomes

$$\frac{d\sigma}{d\Omega}=\frac{(2\pi)^4}{(2J_A+1)}\frac{\mu_\pi}{|\mathbf{k}_\pi|}\sum_{m'_s\nu_A\nu_B}\left|\sum_{jm_j}(\mathscr{N}_j\mu_N\,|\,\mathbf{K}_N\,|\,)^{1/2}\sum_{\substack{\gamma lm_lm_s\\ Lm_LJ_C\nu_C}}\mathscr{C}I^{\mathrm{EDW}}_{Lm_L,lm_l}\right.$$
$$\left.\times[(2\pi)^3\langle-(\mathbf{K}_N+\langle\mathbf{Q}'\rangle);\mathbf{K}_N,\tfrac{11}{22},\tfrac{1}{2}m'_s\,|\,t(\sqrt{s}\,)_{\pi N\to\eta N}\,|\,\mathbf{k}_\pi;-(\mathbf{k}_\pi+\langle\mathbf{Q}'\rangle),\tfrac{1}{2}-\tfrac{1}{2},\tfrac{1}{2}m_s\rangle]\right|^2\ , \tag{A4}$$

where

$$I^{\mathrm{EDW}}_{Lm_L,lm_l}=\int d\mathbf{K}'_N d\mathbf{k}'_\pi d\mathbf{Q}'\Psi^{*(-)}_{\mathbf{K}'_N}(\mathbf{K}'_N)\psi^*_{Lm_L}(\mathbf{Q}'+\beta\mathbf{K}'_N)\phi_{nlm_l}(\mathbf{Q}'+\alpha\mathbf{k}'_\pi)\Phi^{(+)}_{\mathbf{k}'_\pi}(\mathbf{k}'_\pi) \tag{A5}$$

has the meaning of a distorted-wave overlapping function in the eikonal approximation. For computational convenience, it is useful to transform Eq. (A5) into a coordinate-space integration involving cylindrical coordinates. This can be done following the method described in Ref. 28. The result is

$$I^{\mathrm{EDW}}_{Lm_L,lm_l}=(2\pi)\exp[-i(m_L-m_l)\phi_{\hat{\mathbf{K}}_N}](i)^{(m_L-m_l)}$$
$$\times\int b\,db\,dz J_{m_l-m_L}(\beta\,|\,\mathbf{K}_N\,|\,b\sin\theta_{\hat{\mathbf{K}}_N})\exp[i(\alpha\,|\,\mathbf{k}_\pi\,|-\beta\,|\,\mathbf{K}_N\,|\cos\theta_{\hat{\mathbf{K}}_N})z]$$
$$\times D_N(\,|\,\mathbf{K}_N\,|,\cos\theta_{\hat{\mathbf{K}}_N},b,z)D_\pi(\,|\,\mathbf{k}_\pi\,|,b,z)\psi^*_L[(b^2+z^2)^{1/2}]\phi_{nl}[(b^2+z^2)^{1/2}]$$
$$\times\left[\frac{(2l+1)(2L+1)}{(4\pi)^2}\right]^{1/2}\left[\frac{(L-m_L)!(l-m_l)!}{(L+m_L)!(l+m_l)!}\right]^{1/2}P_l^{m_l}[z/(b^2+z^2)^{1/2}]P_L^{m_L}[z/(b^2+z^2)^{1/2}]\ , \tag{A6}$$

with

$$D_N(\,|\,\mathbf{K}_N\,|,\cos\theta_{\hat{\mathbf{K}}_N},b,z)=\exp\left[-i\frac{\mu_N}{|\,\mathbf{K}_N\,|}\int_0^\infty V_{NB}(\bar{L}_N,z+s\cos\theta_{\hat{\mathbf{K}}_N})ds\right] \tag{A7}$$

and

$$D_\pi(\,|\,\mathbf{k}_\pi\,|,b,z)=\exp\left[-i\frac{\mu_\pi}{|\,\mathbf{k}_\pi\,|}\int_{-\infty}^z V_{\pi A}(b,z')dz'\right]\ . \tag{A8}$$

In deriving Eq. (A6), we have used the relations $\psi_{Lm_L}(\mathbf{x})=\psi_L(x)Y_{Lm_L}(\hat{\mathbf{x}})$ and $\phi_{nlm_l}(\mathbf{x})=\phi_{nl}(x)Y_{lm_l}(\hat{\mathbf{x}})$. In Eqs. (A7) and (A8), V_{NB} and $V_{\pi A}$ stand, respectively, for the nucleon-nucleus[25] and pion-nucleus[28] optical potentials. The $J_{m_l-M_L}$ is the Bessel function of order m_l-M_L and $\bar{L}_N$ is an averaged impact parameter of the outgoing proton. We refer to the Appendix of Ref. 28 for the derivation of $\bar{L}_N$ and the geometry used for the eikonal distortion calculation.

[1]T. D. Lee, *Particle Physics and Introduction to Field Theory* (Harwood-Academic, Amsterdam, 1981); J. F. Donoghue and H. Gomm, Phys. Rev. D **28**, 2800 (1983).

[2]A. Duane, D. M. Binnie, L. Camilleri, J. Carr, N. C. Debenham, D. A. Garbutt, W. G. Jones, J. Keyne, I. Siotis, and J. G. McEwen, Phys. Rev. Lett. **32**, 425 (1974); see also T. D. Lee in Ref. 1.

[3]S. A. Coon and B. M. Preedom, Phys. Rev. C **33**, 605 (1986); D. J. Gross, S. B. Treiman, and F. Wilczek, Phys. Rev. D **19**, 2188 (1979).

[4]J. C. Peng, *Hadronic Probes and Nuclear Interactions,* Proceedings of the International Conference on Hadronic Probes and Nuclear Interactions (Arizona State University, 1985), AIP Conf. Proc. No. 133, edited by Joseph R. Comfort, William R. Gibbs, and Barry G. Ritchie (AIP, New York, 1985), p. 255.

[5]P. Berthet, R. Frascaria, J. P. Didelez, Ch. F. Perdrisat, G. Pignault, J. Banaigs, J. Berger, L. Goldzahl, F. Plouin, F. Fabbri, P. Picozza, L. Satta, M. Boivin, and J. Yonnet, Nucl. Phys. **A443**, 589 (1985).

[6]R. S. Bhalerao and L. C. Liu, Phys. Rev. Lett. **54**, 865 (1985).

[7]Q. Haider and L. C. Liu, Phys. Lett. **172B**, 257 (1986); **174B**, 465(E) (1986).

[8]R. Seki, Phys. Rev. C **26**, 1342 (1982); Prog. Theor. Phys. **74**, 511 (1985).

[9]R. Seki and K. Masutani, Phys. Rev. C **27**, 2799 (1983); **27**, 2817 (1983).

[10]R. Seki and K. Wiegand, Annu. Rev. Nucl. Sci. **25**, 241 (1975).

[11]B. Povh, Annu. Rev. Nucl. Part. Sci. **28**, 1 (1978).

[12]R. H. Landau, Phys. Rev. C **27**, 2191 (1983); **28**, 1324 (1983); R. H. Landau and B. Cheng, *ibid.* **33**, 734 (1986).

[13]Y. R. Kwon and F. Tabakin, Phys. Rev. C **18**, 932 (1978).

[14]L. S. Celenza, M. K. Liou, L. C. Liu, and C. M. Shakin, Phys. Rev. C **10**, 398 (1974).

[15]L. C. Liu and C. M. Shakin, Prog. Part. Nucl. Phys. **5**, 207 (1980).

[16]J. M. Blatt and V. F. Weisskopf, *Theoretical Nuclear Physics* (Wiley, New York, 1962).

[17]These results differ slightly from those of Ref. 7 because of an improved numerical integration over the Fermi motion of the nucleons.

[18]L. C. Liu, Phys, Rev. C **17**, 1787 (1978).

[19]L. C. Liu and C. M. Shakin, Nuovo Cimento **53A**, 142 (1979).

[20]M. Beiner, H. Flocard, N. V. Giai, and P. Quentin, Nucl. Phys. **A238**, 29 (1975).

[21]R. H. Landau and A. W. Thomas, Phys. Lett. **88B**, 226 (1979).

[22]L. S. Celenza, L. C. Liu, W. Nutt, and C. M. Shakin, Phys. Rev. C **14**, 1090 (1976).

[23]L. Celenza, L. C. Liu, and C. M. Shakin, Phys. Rev. C **11**, 1593 (1975).

[24]B. A. Watson, P. P. Singh, and R. E. Segel, Phys. Rev. **182**, 977 (1969).

[25]A. K. Kerman, H. McManus, and R. M. Thaler, Ann. Phys. (N.Y.) **8**, 561 (1959).

[26]If the band is very large such that it contains two or more shells that are of different l values but the same j value, e.g., $p_{3/2}$ ($l=1, j=\frac{3}{2}$) and $d_{3/2}$ ($l=2, j=\frac{3}{2}$), then an additional term proportional to $2\,\mathrm{Re}(\tilde{F}\,\tilde{G}^{*})$ will appear in Eq. (3.6).

[27]J. N. Ginocchio, Phys. Rev. C **17**, 195 (1978).

[28]Y. Ohkubo and L. C. Liu, Phys. Rev. C **30**, 254 (1984).

[29]This choice of δ is based on our observation that the η binding energies given by the factorized approximation with $\delta=30$ MeV are in reasonable agreement with the full off-shell results (set 1 of Table I). This value of δ is similar to the one found in pion-nucleus elastic scattering [see, e.g., W. B. Cottingame and D. B. Holtkamp, Phys. Rev. Lett. **45**, 1828 (1980)] and can be understood in the same way (Ref. 15), namely, that the average nuclear binding and Fermi motion amount to about a 30 MeV downward shift of the hadron-nucleon interaction energy $\sqrt{s_j}$.